Plasma Physics and
Controlled Fusion

PURPOSE-LED
PUBLISHING™

PAPER • **OPEN ACCESS**

Proper orthogonal decomposition as an analytical approach to parametrisation of asymmetry and heat flux analysis in the Wendelstein 7-X stellarator

To cite this article: Bartosz Zamorski *et al* 2025 *Plasma Phys. Control. Fusion* **67** 105027

View the article online for updates and enhancements.

You may also like

- A novel diagnostic method for electrons accelerated from relativistic magnetic reconnection via electron spin polarization
L R Yin, Y J Gu, X F Li et al.
- Large time-scale kinetic simulations of counter-propagating plasma shocks in the hohlraum
Xu Zhang, Fan-qi Meng, Wen-shuai Zhang et al.
- A zero order study of the effect of resonances on fast ions measured by FILD in ASDEX Upgrade
P A Zestanakis, G Anastassiou, J Rueda-Rueda et al.

This content was downloaded from IP address 129.13.194.163 on 31/10/2025 at 10:08

OPEN ACCESS
IOP Publishing
Plasma Physics and Controlled Fusion
Plasma Phys. Control. Fusion **67** (2025) 105027 (20pp)
https://doi.org/10.1088/1361-6587/ae1325

Proper orthogonal decomposition as an analytical approach to parametrisation of asymmetry and heat flux analysis in the Wendelstein 7-X stellarator

Bartosz Zamorski[1,*], Marcin Sleczka[1], Marcin Jakubowski[2], Yu Gao[2], Aleix Puig Sitjes[2], Konrad Czerski[1] and the W7X Team[3]

[1] Institute of Physics, University of Szczecin, Wielkopolska 15, Szczecin 70-450, Poland
[2] Max-Planck-Institut für Plasmaphysik, Wendelsteinstraße 1, Greifswald 17491, Germany

E-mail: bartosz.zamorski@usz.edu.pl

Received 26 April 2025, revised 27 September 2025
Accepted for publication 14 October 2025
Published 24 October 2025

Abstract
The complex dynamics of plasma and the heat flux through divertors in stellarator fusion devices, with a focus on the Wendelstein 7-X (W7-X), can be more easily understood by leveraging the proper orthogonal decomposition (POD) method. POD has been used to analyse discharges to identify divertor asymmetries indicative of underlying plasma transport phenomena. It has been demonstrated that the POD method, recognised for its dimension-reduction prowess, can effectively distill high-dimensional datasets into a manageable number of significant modes, facilitating the interpretation of intricate plasma behaviour. The findings reveal that the primary POD modes encapsulate the majority of the significance of the signal, underscoring the asymmetries caused by plasma drifts, and revealing the correlations of the POD modes linked to specific physical phenomena within the reactor vessel. Furthermore, an average symmetrisation parameter has been introduced as a diagnostic tool to quantify symmetry in heat flux deposition, revealing its potential to characterise and mitigate asymmetries.

Keywords: proper orthogonal decomposition, divertor, heat flux, stellarator, Wendelstein 7-X

1. Introduction

The control of heat flux through plasma-facing components (PFCs) remains a critical challenge in magnetic confinement fusion, particularly for steady-state devices such as stellarators. The Wendelstein 7-X (W7-X) (Klinger *et al* 2019), the most advanced stellarator to date, has demonstrated substantial improvements in plasma confinement and the reduction of neoclassical transport, attributable to its quasi-isodynamic (QI) magnetic configuration (Landreman 2011). The heat and power exhaust is realised with the island divertor, which creates a non-axisymmetric distribution of divertor power loads (Jakubowski *et al* 2021) dependent on plasma configuration and plasma parameters. Due to complexity of the non-linear phenomena at the plasma edge it is not always straightforward to model transport in the island divertor, therefore it is important to be able to gain insights into dependence of the power loads on plasma parameters by other means (Pedersen *et al* 2019a, Niemann *et al* 2020a, Grulke *et al* 2024).

[3] See Grulke *et al* 2024 (https://doi.org/10.1088/1741-4326/ad2f4d) for the W7-X Team.
[*] Author to whom any correspondence should be addressed.

Original Content from this work may be used under the terms of the Creative Commons Attribution 4.0 licence. Any further distribution of this work must maintain attribution to the author(s) and the title of the work, journal citation and DOI.

© 2025 The Author(s). Published by IOP Publishing Ltd

Only the standard W7-X configuration is QI-optimised; the alternative edge-ι settings (e.g. low-ι 5/6 and high-ι 5/4) are not QI-optimised by design, although some may exhibit favourable transport through reduced turbulence. In this paper we primarily analyse the standard and low iota configuration for the detailed proper orthogonal decomposition (POD) results, while additional discharges across high-mirror or iota scan settings are included in the survey to demonstrate methodological robustness.

Real-time diagnostics, such as infrared (IR) thermography, play a critical role in monitoring heat flux distribution, providing high-resolution thermal imaging of the divertor surfaces, and identifying asymmetries and hotspots. However, advanced data analysis techniques are required to fully interpret the complex heat flux patterns captured by these diagnostics (Sitjes *et al* 2018, Jakubowski *et al* 2021).

This study employs POD to reduce high-dimensional thermographic data into orthogonal modes, representing the most significant spatial and temporal features of the heat flux distribution. By isolating dominant heat flux patterns, POD enables a clearer understanding of how the magnetic topology influences heat deposition on the divertor plates, providing a reduced-order representation of the underlying physical processes (Mendez *et al* 2019, Kriete *et al* 2023). A symmetrisation parameter is introduced to quantify the asymmetry between the upper and lower POD modes, offering a diagnostic tool to assess power load symmetrisation and optimise divertor performance under varying plasma conditions (Pisano *et al* 2020).

All analysed discharges employed a constant electron cyclotron resonance heating (ECRH) profile without changes during the discharge. Consequently, observed temporal features in the POD modes can be ascribed to intrinsic plasma dynamics-such as evolving density, bootstrap current development, or transport phenomena-rather than heating modulations. This ensures that the extracted modes are representative of physical effects rooted in the magnetic configuration and plasma behaviour, not external forcing.

Correlations between specific POD modes and key plasma parameters, such as plasma density, electron and ion temperature profiles, and toroidal currents, provide further insight into how plasma conditions influence heat flux dynamics, with implications for mitigating asymmetries and improving power exhaust in stellarator configurations (Lazerson *et al* 2018, Gao *et al* 2019, Corre *et al* 2021). Experimental data from the operational campaigns OP1.2 and OP2.1, obtained by IR thermography and real-time image processing, form the foundation for the development of predictive models to manage heat loads in future high-power, long-pulse operations (Sitjes *et al* 2018, Niemann *et al* 2020a).

While IR thermography has been extensively used for mapping heat flux distributions in fusion devices, this study represents the first time that the POD method is utilised to decompose these data into spatial and temporal modes. This novel approach enables us to extract dominant features in the heat flux patterns and simultaneously correlate them with multiple key plasma parameters.

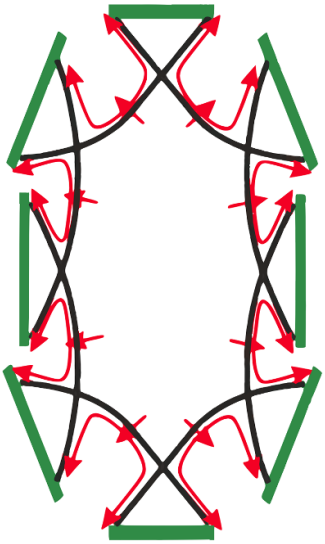

Figure 1. Illustration of the island divertor concept, where the island count, denoted as n, varies across different stellarator devices. In the case of the W7-X device, n is selectable within the range of 4–6, with $n = 5$ as the conventional choice. Reproduced from Feng *et al* (2006). © 2006 IAEA, Vienna.

2. Heat Transport in Wendelstein 7-X

Heat transport in Wendelstein 7-X (W7-X) is governed by the island divertor concept, which utilises magnetic islands at the plasma edge to manage heat and particle exhaust. These islands, formed by the unique three-dimensional magnetic configuration of W7-X, intersect with the divertor plates as presented in figure 1, defining strike lines where heat flux is deposited (McCormick *et al* 2003, Feng *et al* 2006). The magnetic configuration is characterised by a low-shear edge, allowing for extended connection lengths and efficient parallel heat transport along magnetic field lines.

The rotational transform ι at the edge determines the size and positioning of magnetic islands, with configurations such as low-iota ($\iota \approx 5/6$) and high-iota ($\iota \approx 5/4$) modulating the heat flux distribution across the divertor targets (Andreeva *et al* 2022).

These islands serve to channel heat exhaust from the plasma boundary, minimising localised heat accumulation by guiding heat flux to defined divertor areas. The five-fold symmetry of W7-X, along with the adjustable edge rotational transform, allows for flexible control of the heat distribution across the divertor targets, which are presented in figure 2.

During Operation Phase 1.2b, uncooled graphite Test Divertor Units (TDUs) were used to handle heat fluxes exceeding 10 MW m^{-2} without active cooling, while the subsequent high-heat-flux (HHF) divertor in OP2.1 introduced water-cooling for sustained operation under higher power scenarios (Wurden *et al* 2018, Kriete *et al* 2023, Grulke *et al* 2024). These magnetic islands enhance exhaust management by isolating the scrape-off layer (SOL) and maintaining plasma purity in the core through effective separation of recycling neutral particles.

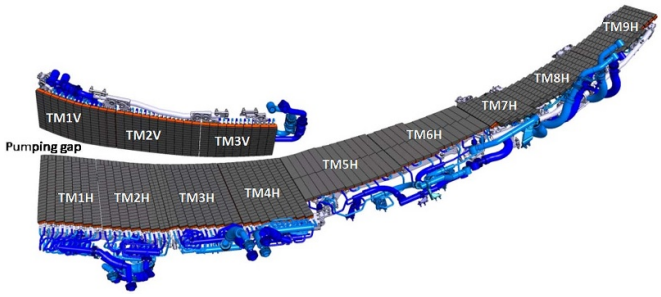

Figure 2. The divertor surface spans 5 m in length and 1 m in width, comprising several target modules: vertical targets (TM1v–TM3v), low-iota targets (TM1h–TM4h), low-load targets (TM5h–TM6h), and high-iota targets (TM7h–TM9h). Reproduced from Puig Sitjes *et al* (2021). CC BY 4.0.

Compared with OP1.2b TDUs, the OP2.1 water-cooled HHF targets differ in thermal inertia and surface emissivity history, which can affect IR camera absolute calibration and response time. Our POD pipeline operates on detrended, mean-subtracted matrices and therefore is primarily sensitive to coherent spatio-temporal variance, not absolute heat-flux scale. This limits the impact of modest inter-phase calibration differences on the extracted leading modes. In the analysis where only the mode structure is critical to the discharge analysis, the scale differences do not alter the observable conclusions.

Connection lengths (L_c) within the SOL play a crucial role in governing the efficiency of heat transport. In W7-X, L_c in the island SOL can range from 450 to 1700 m (Niemann *et al* 2020b). These longer connection lengths allow heat and particle fluxes to travel parallel to the magnetic field, reducing the risk of localised overheating and ensuring an even distribution of heat across the divertor.

The radial power fall-off length, Λ_q, in W7-X typically ranges from 9 to 14 mm, significantly wider than those observed in tokamak H-mode operations, which reflects the lower magnetic shear and broader heat flux profile in the stellarator configuration (Pedersen *et al* 2019b). Additionally, $\boldsymbol{E} \times \boldsymbol{B}$ drift effects create asymmetries in the heat flux distribution, leading to lack of symmetry between the upper and lower divertor targets. These asymmetries are influenced by the edge magnetic topology and are modulated by variations in plasma density and magnetic configuration (Hammond *et al* 2019, Kriete *et al* 2023).

Real-time monitoring of heat flux in W7-X is achieved using IR thermography, which provides high-resolution temperature maps of the divertor surfaces. These measurements are processed through the THEODOR code to calculate heat flux based on surface temperature data (Herrmann *et al* 1995, Gan *et al* 2013). During the operational campaigns, IR thermography plays a critical role in mapping the strike lines and heat flux distributions. We clarify that this estimate applies to the fraction of non-radiated power: for example, a substantial fraction of the total heating power-often between 30%–50% is radiated away from the plasma volume, then of the remaining power, up to 95% is observed on the divertor targets (Pedersen *et al* 2019b).

The island divertor configuration in W7-X demonstrated robust heat-handling capabilities during long-pulse operations, with sustained plasma attachment preventing excessive thermal stress on the PFCs. These diagnostics also helped correct for magnetic error fields, improving the alignment between predicted and observed strike-line geometries, thereby optimising heat load distribution (Hammond *et al* 2019, Niemann *et al* 2020a).

POD, as introduced in section 3, offers a powerful tool for analysing complex heat flux dynamics by isolating dominant modes in the thermal data. This reduced-order analysis has been instrumental in identifying correlations between specific POD modes and plasma parameters such as density and temperature profiles, helping to predict heat flux behaviour and prevent localised overheating.

3. POD

POD, also called the Karhunen–Loéve expansion is a mathematical technique employed to analyse complex, high-dimensional datasets by reducing them to their most significant components, or modes. In plasma physics, where the behaviour of complex systems generates large quantities of data, POD is used to decompose this data into a series of orthogonal spatial modes, each modulated by time-dependent coefficient. This decomposition simplifies the study of complex systems, such as the heat flux distribution on PFCs, by isolating the dominant features and patterns that drive the system's behaviour (Tanaka *et al* 2018).

POD decomposes a given signal into an infinite number of orthogonal spatial modes $\boldsymbol{\Phi_k}(x)$ and corresponding temporal coefficients $a_k(t)$, which represent the temporal evolution of each spatial mode:

$$\hat{\mathbf{I}}(x,t) = \sum_{k=1}^{\infty} a_k(t)\,\boldsymbol{\Phi_k}(x)\,. \tag{1}$$

This decomposition allows the separation of spatial structures and temporal behaviour, offering a clear interpretation of the physical phenomena governing plasma dynamics.

To identify the spatial modes, one solves the eigenvalue problem associated with the covariance matrix:

$$\mathbf{C}\boldsymbol{\Phi_k}(x) = \lambda_k \boldsymbol{\Phi_k}(x)\,, \tag{2}$$

where $\boldsymbol{\Phi_k}(x)$ represents the kth spatial eigenfunction, or mode, and λ_k is the corresponding eigenvalue. The eigenvalues are ordered such that $\lambda_1 \geqslant \lambda_2 \geqslant \cdots \geqslant \lambda_\infty$, indicating that the first few modes capture the largest portion of the variance in the dataset. The eigenvalue λ_k quantifies the contribution of the kth mode to the total system variance.

The temporal coefficients $a_k(t)$, which describe the evolution of each mode in time, are obtained by projecting the original fluctuation dataset $\hat{\mathbf{I}}(x,t)$ onto the corresponding spatial mode

$$a_k(t) = \int \hat{\mathbf{I}}(x,t)\, \mathbf{\Phi_k}(x)\, \mathrm{d}x. \tag{3}$$

This projection isolates the contribution of each mode to the overall dynamics, allowing for the study of how different spatial patterns evolve over time. In fusion devices like W7-X, where the perpendicular transport is defined to a large degree by turbulence and parallel transport by convection/-conduction and drifts, these spatial modes can correspond to coherent structures in the SOL or localised heating patterns on the divertor (Gao *et al* 2019, Niemann *et al* 2020b).

In practical applications, the infinite sum in the POD decomposition is truncated to include only the first k modes, where k is chosen such that the retained modes capture a desired proportion of the total variance, typically defined by the cumulative sum of the eigenvalues:

$$\sum_{i=1}^{k} \lambda_i \Big/ \sum_{i=1}^{\infty} \lambda_i \geqslant \text{Threshold}. \tag{4}$$

By retaining only the leading modes, POD significantly reduces the complexity of the system while maintaining its most important features. This reduced-order model is particularly useful in scenarios requiring real-time analysis or control, such as divertor heat flux management in long-pulse plasma operations (Pisano *et al* 2021, Grulke *et al* 2024).

4. Understanding strike line characteristics and divertor asymmetries using POD

In the W7-X, a QI stellarator (Landreman 2011) with a five-fold modular structure, the coil systems are categorised into three distinct groups: superconducting magnets, trim coils, and control coils (CCs) (Rummel *et al* 2019). The CC system comprises of ten uniform 3D-shaped CCs, strategically positioned behind the baffle plates of respective divertor units as presented in figure 3. Their primary functions include the correction of error fields and to vary the position and the geometry of the strike lines on the divertor surface through changing the magnetic island size and position (Jauregi *et al* 2003, Ślęczka *et al* 2018). The strike line resulting from the plasma-divertor interactions is recorded by the IR systems. The data from the cameras is calibrated and converted into a temperature map. These maps were then utilised by the 2D THEODOR code for calculating the heat flux density. Subsequent analyses focus on various heat flux parameters, including heat flux profiles and the wetted area (Niemann *et al* 2020a). The profile of heat flux on the divertor element is determined through the resolution of a two-dimensional heat diffusion equation, utilising the explicit Euler method for computation (Herrmann *et al* 1995)

$$\rho c_p \frac{\partial T}{\partial t} = \nabla\left(\kappa \nabla T\right), \tag{5}$$

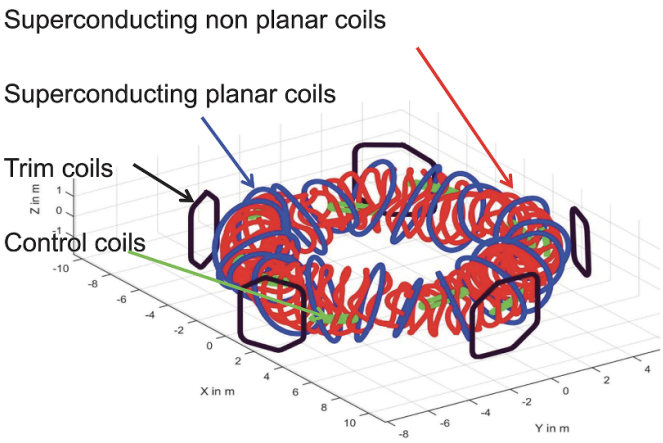

Figure 3. Magnet systems of Wendelstein 7-X: non-planar coils (red), planar coils (blue), trim coils (black), and control coils (green). Reproduced from Rummel *et al* (2019). CC BY 4.0.

where ρ is the volumetric mass density, c_p the specific heat capacity and κ the heat conductivity. To simplify the analysis of the mean heat flux, the mean divertor approach has been used, treating upper and lower divertor modules separately. In this method, heat flux is averaged across the respective divertor modules. The mean heat flux analysis offers insights into the deposition of heat flux across the divertor surface and its variation during a discharge.

The selected discharge, 20 180 828.030 in low-ι magnetic configuration, serves as a model for analysing heat flux dynamics in the W7-X stellarator. This discharge was chosen due to the stability of key plasma parameters, including ECRH power (P_{ECRH}), electron density (n_{e}), and electron temperature (T_{e}). These steady conditions are ideal for isolating and analysing heat flux distribution and identifying asymmetries under quasi-steady-state conditions. Figure 4 presents the temporal evolution of key plasma parameters. Moreover, the target modules, which are specialised components integrated within the W7-X divertor system are strategically positioned to measure the localised heat flux impacting the plasma-facing surfaces, allowing for segmentation of essential data on energy deposition. This precise measurement facilitates the analysis of spatial asymmetries in heat flux, which is critical for evaluating the performance of the magnetic configuration (Boscary *et al* 2021). Figure 5 shows the mean heat flux recorded on target modules TM1h through TM4h. Although all four target modules are displayed, only TM1h to TM3h will be used for the POD analysis, as they receive the most significant and stable heat fluxes, while TM4h experiences minimal heat flux. This selection of the target modules included in the analysis is based on the configuration of magnetic islands and strike lines in W7-X, which directs the majority of heat flux to TM1h through TM4h. These target modules capture the essential spatial and temporal patterns and reveal asymmetries between the upper and lower divertors, making them ideal for analysing drift-induced transport phenomena.

The selection of target modules for POD analysis is discharge-specific and depends heavily on the magnetic configuration, plasma conditions, and divertor geometry. In other

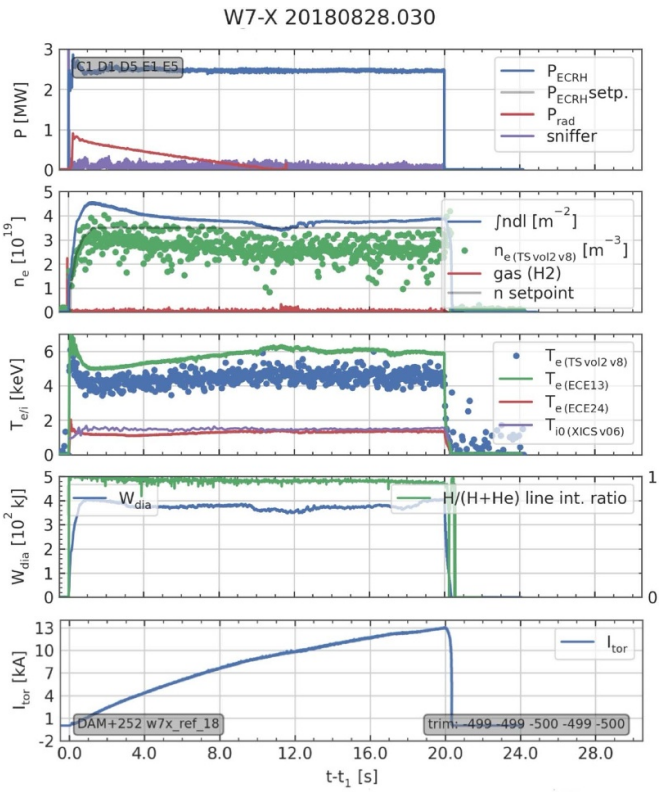

Figure 4. Temporal evolution of key plasma parameters in 20 180 828.030 discharge: the graph presents a stable discharge profile with parameters such as P_{ECRH}, n_{e}, T_{e}, and impurity content remaining constant. Notably, I_{tor} exhibits a monotonic increase.

discharges, particularly those with different magnetic field topologies, the choice of target modules may change. For instance: in configurations where strike lines are distributed unevenly across the divertor, target modules experiencing the most intense heat flux should be prioritised; for discharges with highly dynamic or transient behaviours, it may be necessary to select target modules that capture rapid changes in heat flux over time; in discharges aimed at exploring symmetry or specific divertor cooling strategies, target modules from both high-heat and low-heat regions may be chosen to provide a more balanced view of the divertor performance.

Ultimately, the selection of target modules should consider their relevance to the physical phenomena under investigation, ensuring that they provide a representative dataset for analysing heat flux patterns and asymmetries. For discharge 20 180 828.030, TM1h through TM3h meet these criteria, as they not only capture the dominant heat flux dynamics but also provide insight into the asymmetries associated with plasma drifts and magnetic topology effects. By analysing these heat flux values independently of plasma parameter trends, we focus specifically on spatial and temporal heat flux behaviours which emerge under steady plasma conditions. This approach enables a targeted investigation of the transport phenomena shaping heat deposition on the W7-X divertor, which can vary significantly depending on the experimental goals and operational configurations of other discharges.

One key feature of this discharge is the steady increase in the toroidal current, which exhibits a smooth, gradual rise over the course of the experiment, reaching a maximum value of 13 kA. This steady evolution of the toroidal current plays an important role in influencing the magnetic topology of the plasma, impacting the position and intensity of strike lines on the divertor plates, through the modification of edge plasma iota (ι) and thus the magnetic island position. This evolution aligns with the changes in mean heat flux across the selected target modules. By analysing these parameters together, we establish a comprehensive view of the plasma's influence on heat flux dynamics, particularly in regions susceptible to drift-driven asymmetries (Hammond *et al* 2019, Kriete *et al* 2023). Figure 6 shows an averaged divertor surface map, presenting the strike line of the mean heat flux deposited on the divertor surface. This strike line provides a spatial context for understanding heat flux patterns across different regions of the divertor, visually illustrating areas of high and low heat load. QI optimisation reduces, but does not eliminate, neoclassical bootstrap drive; in addition, net toroidal current can arise from ECCD balance and edge conditions. The measured I_{tor} therefore reflects a small but finite bootstrap contribution and auxiliary-current effects. Its steady rise modifies the edge ι-profile and hence the island geometry.

Both the beginning and the end of the discharge were excluded from the analysis due to the transient behaviour typically observed during the initial ramp-up and final decay phases. By focusing on the central, steady-state portion of the discharge from $t_{\mathrm{start}} = 0.3$ to $t_{\mathrm{end}} = 19$ s, where plasma parameters are fully developed and stable, the analysis can better isolate the effects of the evolving toroidal current on heat flux dynamics and divertor performance. This careful selection of the discharge time window enhances the reliability of the data, minimising the influence of transient phenomena such as rapid changes in edge density or shifts in plasma position in order to simplify this first analysis. The stable conditions during this discharge, combined with the controlled increase in toroidal current, provide an excellent opportunity to study the effects of current-driven modifications to the magnetic island structure.

The above discharge, 20 180 828.030 has then been analysed with the use of POD (Pearson 1901, Berkooz *et al* 1993, Tanaka *et al* 2018, 2019). For the POD analysis, a data matrix has been constructed from the fluctuation components of the composed data matrix $\hat{\mathbf{I}}(x,t) = \mathbf{I}(x,t) - \bar{\mathbf{I}}(x,t)$ of the heat flux on selected divertor modules, TM1h through TM3h. By structuring the matrix to separately analyse upper and lower divertors, we can preserve and investigate asymmetrical patterns. Figure 7 illustrates the original data matrix, where the structured arrangement enables a focused analysis on the spatial variations in heat flux. This matrix configuration is advantageous in the stellarator geometry, as the non-axisymmetric magnetic fields of W7-X promote drift-induced asymmetries that manifest in the form of differential heat and particle fluxes. By arranging the data in a matrix suited for POD, we effectively set the foundation for a decomposition that reveals these underlying drift dynamics.

The eigenvalues, illustrated in figure 8, represent the variance contribution of each mode, with the first two modes

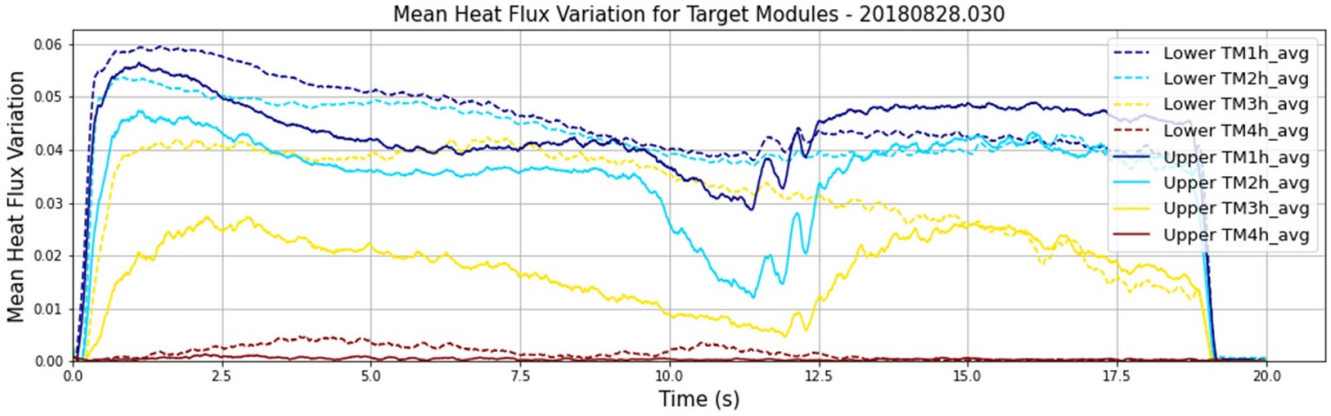

Figure 5. Mean heat flux variation over time for target modules (TM1h–TM4h) in discharge 20 180 828.030, separated by upper and lower divertor regions. The plot shows average heat flux trends for each target module, revealing significant differences in heat deposition between the upper and lower divertors.

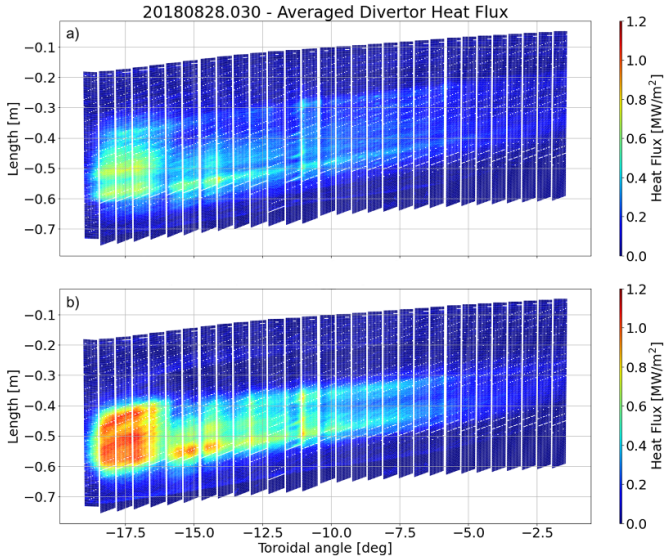

Figure 6. Averaged divertor surface map showing the strike line of mean heat flux deposition across the divertor surface in discharge 20 180 828.030. In part (a), the upper module of the divertor is displayed, while in part (b), the lower module of the divertor is shown. The maps highlight regions of concentrated heat load, revealing the asymmetric distribution of heat flux between the upper and lower divertor modules, consistent with edge drifts (Hammond *et al* 2019).

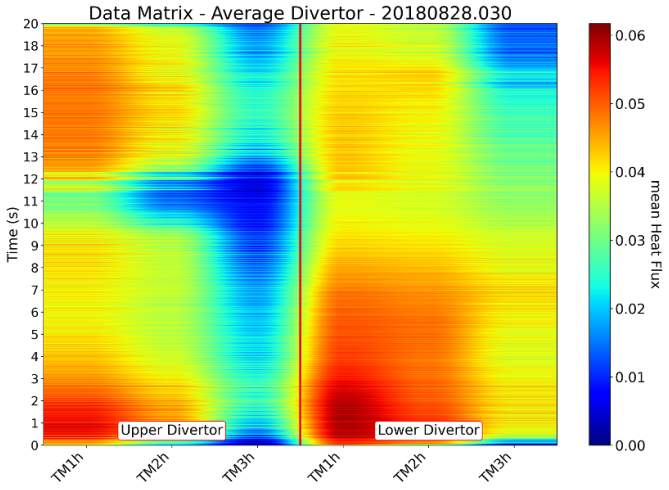

Figure 7. Data matrix for POD analysis of mean heat flux matrix depicting the spatial distribution of energy deposition on divertor surfaces, vital for understanding the thermal load patterns, illustrating the extent of plasma–material interaction regions, critical for assessing the distribution and management of heat loads across the divertor surfaces.

collectively capturing a significant portion of the total variance (52.6% and 33.9%, respectively), amounting to 86.5%. This high cumulative contribution demonstrates that these two modes encapsulate the dominant patterns in heat flux distribution, while the remaining modes contribute to finer, more localised features.

The first spatial mode $\mathbf{\Phi_1}$, shown in figure 9, captures a relatively symmetric distribution of heat flux across the divertor modules. This pattern reflects a baseline heat flux distribution, indicative of a balanced deposition profile across the selected target modules. The corresponding temporal coefficient $a_1(t)$ presented in figure 10 shows significant temporal evolution, including a pronounced rise around $t = 11 - 12$ s. This dynamic behaviour suggests that this mode is strongly influenced by variations in heating. This observation will be explored further in a later section of this work, where correlations with plasma parameters will be analysed to better understand the relationship between heating power and the temporal evolution of this mode.

The second spatial mode $\mathbf{\Phi_2}$, shown in figure 9, captures a prominent asymmetry between the upper and lower divertors, corresponding to the baseline heat flux pattern observed in figure 7, where we can see that the lower module of the divertor receives a significantly larger heat flux load.

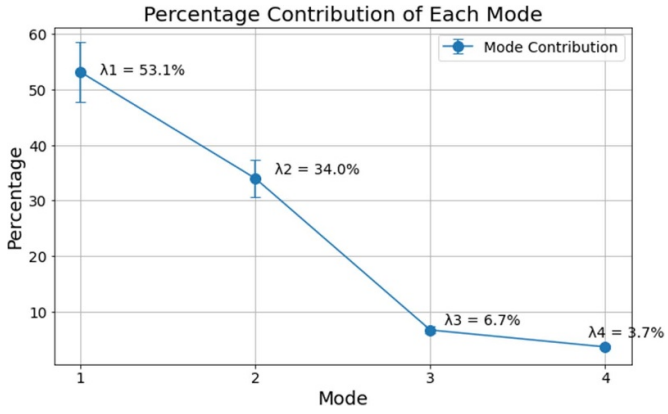

Figure 8. The percentage contribution $\lambda_k / \sum_{i=1}^{n}$ across various POD modes. Each mode's contribution, in descending order of magnitude, is essential for optimising mode selection in data set reconstruction. Additionally, beyond a certain point, further modes have negligible effects, as their values fall below the level of experimental measurement.

However, the rapid increase in the temporal coefficient $a_2(t)$ presented in figure 10 during the latter part of the discharge indicates a dynamic evolution of this mode. This suggests that the observed asymmetry is not merely a steady-state feature but is instead influenced by time-dependent plasma processes, possibly linked to changes in magnetic topology, confinement properties, or drift-induced transport phenomena. The dominant drifts in W7-X are the poloidal and radial $E \times B$ drifts (Hammond *et al* 2019), with the poloidal one prevailing at low densities and the radial one at higher densities (Kriete *et al* 2023). Here, due to the relatively low density, we mainly observe poloidal drifts, which are determined by the electron temperature distribution at the divertor $(V_\mathrm{p} \approx 3T_\mathrm{e,divertor}/e)$, while the radial electric field E_r depends on the potential distribution. This transient behaviour emphasises the importance of considering temporal dynamics when interpreting the spatial asymmetries in heat flux distribution.

Higher-order modes, such as $\mathbf{\Phi_2}$ and beyond, reflect progressively finer spatial features, potentially indicative of transient or localised plasma phenomena. The temporal coefficients for these modes show higher variability, suggesting that these modes may correspond to non-stationary processes. By combining any two modes through weighted summation based on λ_i and λ_j, such that

$$\mathbf{\Phi}_{i+j} = \frac{\lambda_i \mathbf{\Phi}_i + \lambda_j \mathbf{\Phi}_j}{\lambda_i + \lambda_j},$$

one can approximate complex effects that span multiple spatial and temporal scales, thereby capturing interactions that would be obscured in single-mode analysis. This approach underscores the adaptability of POD in isolating and interpreting physical features which may mathematically span various modes, however represent one physical effect embedded within a high-dimensional dataset.

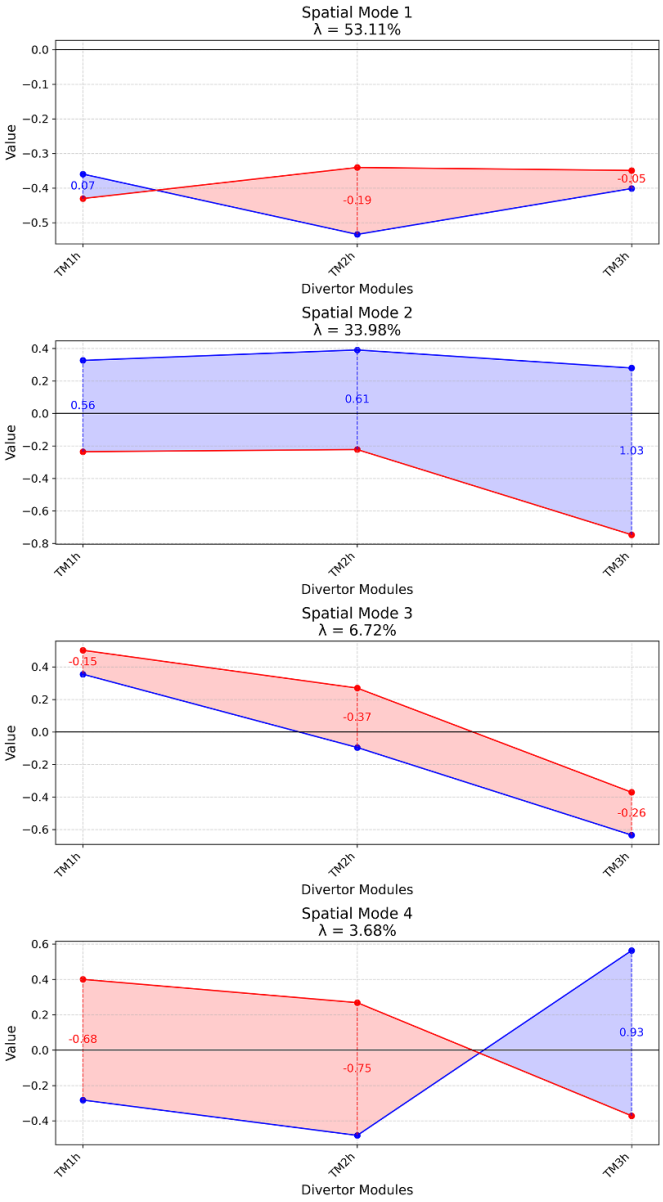

Figure 9. Spatial modes derived from the POD analysis for discharge 20 180 828.030, showing the distribution of values across target modules TM1h–TM3h for the upper (red) and lower (blue) divertors. The symmetrisation parameter values are presented between the upper and lower components with appropriate shading. Spatial Mode 1 $(\mathbf{\Phi_1})$ shows a relatively symmetric heat flux distribution influenced by heating variations. Spatial Mode 2 $(\mathbf{\Phi_2})$ captures a pronounced asymmetry with dynamic temporal evolution, linked to time-dependent plasma processes. Higher modes reflect localised fluctuations and transient plasma behaviours. λ values obtained from figure 8.

5. Average symmetrisation parameter (ς)

In the context of heat flux distribution analysis, symmetry between the upper and lower divertors plays a crucial role in understanding and optimising PFC performance in stellarators such as W7-X. In particular, asymmetries in the heat flux are

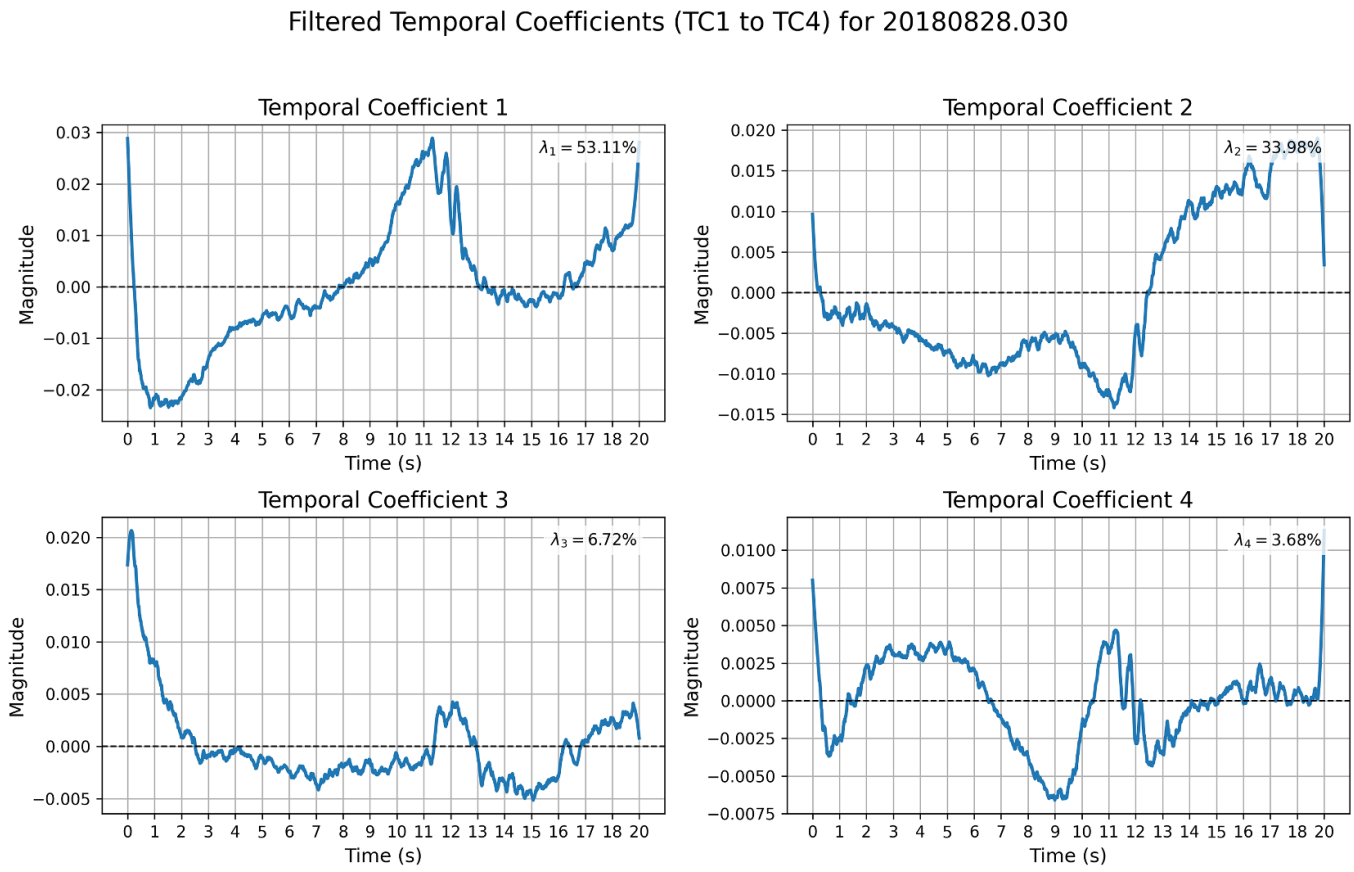

Figure 10. Temporal coefficients derived from the POD analysis for discharge 20 180 828.030. Each plot presents the temporal coefficient of one of the first four individual POD modes, with its corresponding eigenvalue (λ_i) representing the variance contribution. Temporal coefficients $a_1(t)$ $(\lambda_1 = 52.58\%)$ and $a_2(t)$ $(\lambda_2 = 33.90\%)$ capture the dominant temporal dynamics of heat flux, while coefficients $a_3(t)$ and $a_4(t)$ reflect higher-frequency, localised fluctuations contributing less variance. This decomposition provides a detailed view of the temporal behaviour of each mode, offering insights into how these independent components influence the heat flux distribution on the divertor over time.

often indicative of drift-driven transport phenomena, which are shaped by the interaction of radial electric fields, density gradients, and the three-dimensional magnetic topology of the stellarator. To quantitatively assess this asymmetry, the average symmetrisation parameter (ς) is introduced, a metric designed to capture the degree of symmetry in heat flux contributions across the divertor surfaces. The average symmetrisation parameter has been defined as:

$$\varsigma = \frac{\sum_{k=1}^{N} \lambda_k \left(\overline{\boldsymbol{\Phi}_{\boldsymbol{k}}^{\boldsymbol{lower}}} - \overline{\boldsymbol{\Phi}_{\boldsymbol{k}}^{\boldsymbol{upper}}} \right)}{\sum_{k=1}^{N} \lambda_k},$$

where $\boldsymbol{\Phi}_{\boldsymbol{k}}^{\boldsymbol{upper}}$ and $\boldsymbol{\Phi}_{\boldsymbol{k}}^{\boldsymbol{lower}}$ are the values of the kth spatial mode respectively for the upper and lower divertor modules, $\overline{\boldsymbol{\Phi}_{\boldsymbol{k}}^{\boldsymbol{upper}}}$ and $\overline{\boldsymbol{\Phi}_{\boldsymbol{k}}^{\boldsymbol{lower}}}$ are the mean of the kth spatial mode values respectively for the upper and lower divertor modules, λ_k is the eigenvalue associated with the kth mode, representing the variance contribution of the mode and N is the total number of spatial modes considered in the calculation.

This parameter obtains the eigenvalue-weighted asymmetry between the upper and lower divertors, normalised by the sum of all eigenvalues. The symmetrisation parameter quantifies the net asymmetry in the spatial distribution of heat flux, weighted by the contribution of each mode to the total variance. The parameter's value has the following physical implications:

- $\varsigma > 0$: The lower divertor receives a greater average heat flux contribution from the spatial modes compared to the upper divertor.
- $\varsigma < 0$: The upper divertor receives a greater average heat flux contribution than the lower divertor.
- $\varsigma \approx 0$: A balanced or symmetric heat flux distribution between the upper and lower divertors.

By incorporating the eigenvalues (λ_k) into the calculation, ς ensures that modes with higher variance contributions (i.e. those that capture more significant features of the heat flux distribution) have a proportionally larger impact on the overall measure of symmetry. Furthermore, in figure 9, the symmetrisation parameter values for individual pairs of $\boldsymbol{\Phi}_{\boldsymbol{k}}$ points (upper and lower divertor contributions) are presented. These values are shown as vertical distances between corresponding points on the upper and lower divertor curves, visually highlighting the local asymmetry in each mode.

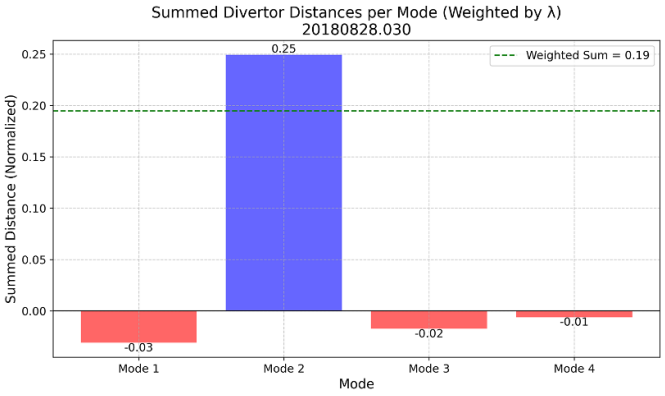

Figure 11. Average symmetrisation parameter (ς) per mode, for discharge 20 180 828.030. The bars represent the normalised asymmetry in spatial mode contributions, with negative values (red) indicating higher contributions from the upper divertor and positive values (blue) indicating dominance of the lower divertor. The horizontal dashed line presents the overall $\varsigma = 0.19$ for this discharge, reflecting a net asymmetry favouring the lower divertor. This visualisation highlights the dominant role of certain modes in shaping the overall heat flux distribution asymmetry.

In order to visualise the contributions to ς, a histogram (figure 11) of the weighted asymmetries $\lambda_k(\overline{\mathbf{\Phi}_k^{lower}} - \overline{\mathbf{\Phi}_k^{upper}})$ can be generated. This histogram highlights the relative importance of each mode in determining the overall asymmetry. A horizontal line indicating the value of ς provides a clear summary of the net symmetry or asymmetry in the system. Additionally, figure 9 presents the vertical distances between the upper and lower divertor values for each spatial mode $\mathbf{\Phi}_k$, providing a direct visualisation of the local asymmetry that contributes to the symmetrisation parameter. This granular representation complements the histogram by showing the pointwise contributions to the overall asymmetry.

6. Correlating plasma parameters with POD temporal Coefficients

The analysis of correlations between plasma parameters and the POD temporal coefficients reveals key physical insights into the dynamics of heat flux distribution in the W7-X stellarator. Specifically, the relationships of the first two temporal coefficients $a_1(t)$ and $a_2(t)$ with line-integrated electron density (n_e) and toroidal plasma current (I_{tor}) highlight the distribution of physical effects across modes and their underlying causes. These correlations are visualised in figure 12, where plasma parameters are mapped onto a unit circle based on their correlation with $a_1(t)$ (x-axis) and $a_2(t)$ (y-axis).

As shown in both figure 12 the first temporal coefficient $a_1(t)$ exhibits a strong correlation with the line-integrated electron density (n_e), labelled (int n dl) in the plot, $(r = 0.729)$. This suggests that the dominant heat flux patterns are strongly influenced by density-driven effects, such as radial particle transport and associated drifts in the plasma edge. Furthermore, the correlation becomes even stronger when $a_1(t)$ is combined with $a_2(t)$ as $a_{1+2}(t)$, $(r = 0.861)$. This observation indicates that the physical effect associated with

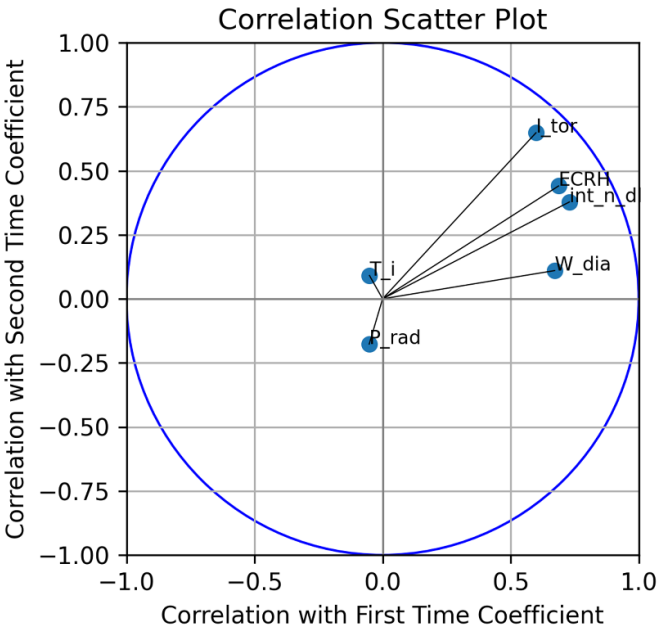

Figure 12. Correlation scatter plot between plasma parameters and the first two temporal coefficients from POD analysis. The plot illustrates the degree of linear correlation between operational plasma parameters, such as ion temperature (T_i), radiation (P_{rad}), and bootstrap current, with the primary temporal coefficients derived from the Proper Orthogonal Decomposition of divertor heat load data. The encapsulating circle represents the unit correlation boundary, emphasising the tight clustering of most parameters and indicating their potential interdependencies during the discharge process in the W7-X Stellarator.

density-driven transport is spread across the first two modes, with $a_1(t)$ capturing the bulk of the steady-state behaviour and $a_2(t)$ reflecting dynamic adjustments or secondary effects. This dual-mode behaviour likely reflects the interaction of steady-state density gradients and transient effects such as fluctuations in edge transport or the influence of magnetic island structures.

The second temporal coefficient $a_2(t)$, which represents secondary features in the heat flux dynamics, shows a strong correlation with the toroidal plasma current (I_{tor}), $(r = 0.648)$. This is visually represented in figure 12, where I_{tor} aligns more strongly with $a_2(t)$ compared to $a_1(t)$.

The influence of I_{tor} on $a_2(t)$ reflects the role of toroidal current evolution in modifying the edge magnetic topology, particularly in the vicinity of magnetic islands and strike line positions. Changes in the I_{tor} can shift the magnetic field configuration, affecting the spatial and temporal distribution of heat flux on the divertor surfaces. The relatively weaker correlation of I_{tor} with $a_1(t)$ further supports the interpretation that I_{tor} influences dynamic, rather than steady-state, effects.

7. Reconstruction of the POD Modes

Reconstruction is a critical step in validating the POD methodology and interpreting the spatial and temporal dynamics of heat flux distribution. By reconstructing the heat flux signal

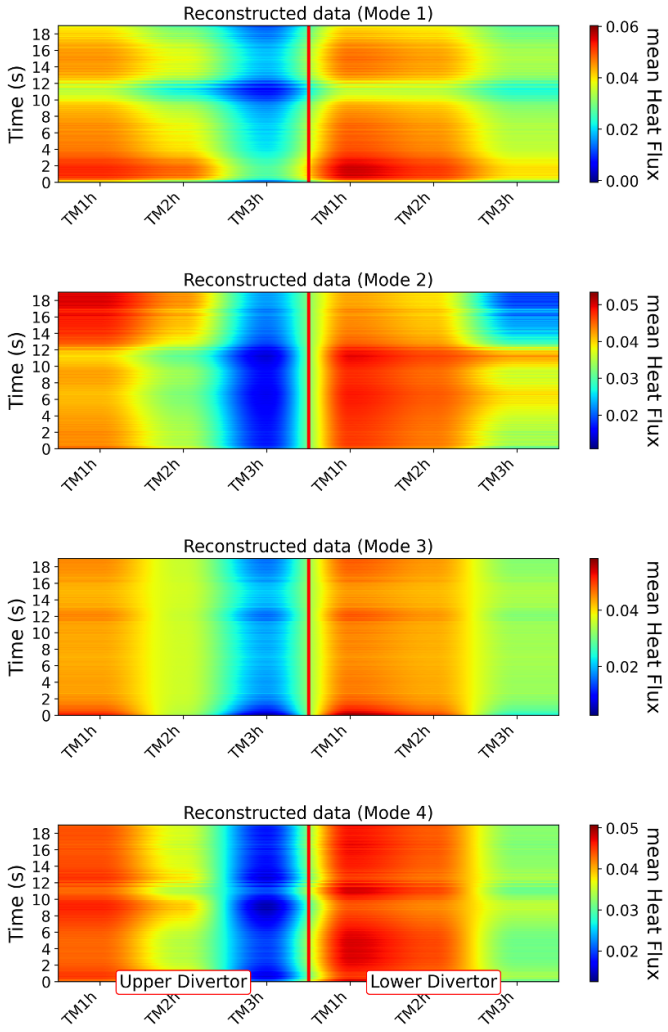

Figure 13. Reconstructed heat flux data for the first four POD modes for discharge 20 180 828.030, showing the temporal evolution of mean heat flux across target modules TM1h–TM3h in the upper and lower divertors. Mode 1 captures the dominant asymmetry in heat flux distribution, consistent with the primary drift-induced transport effects. Mode 2 highlights additional asymmetries and broader-scale patterns, while Modes 3 and 4 reveal higher-frequency fluctuations and localised features. The colour scale indicates the mean heat flux intensity, with warmer colours representing higher fluxes. These reconstructions demonstrate how each mode contributes uniquely to the overall heat flux dynamics.

from a subset of POD modes, it is possible to assess the accuracy of the decomposition process and gain deeper insights into the physical phenomena represented by individual modes. The reconstructed heat flux contributions for the first four modes, which collectively fully reconstruct the original data set, have been presented in figure 13 and the implications of their spatial and temporal structures will be discussed below.

The reconstructions highlight the asymmetry between the upper and lower divertors, particularly in Modes 1 and 2. These asymmetries align with the observations of the average symmetrisation parameter (ς) discussed previously. The strong contributions from Modes 1 and 2, combined with their correlations to n_e and I_{tor}, underscore the role of density-driven transport and magnetic topology changes in shaping these asymmetries. The distribution of physical effects across multiple modes is further emphasised by the combined correlation of $a_{1+2}(t)$ with n_e, which is stronger than the correlation of $a_1(t)$ alone. This suggests that the interplay between steady-state transport and dynamic adjustments contributes significantly to the observed heat flux patterns. The reconstructed data for Modes 1 and 2 collectively describe the large-scale, dominant behaviours, while Modes 3 and 4 add finer-scale features and transient effects. These interactions provide a comprehensive picture of the heat flux dynamics, highlighting the multiscale nature of the physical phenomena at play.

The reconstructed signal achieves a near-perfect match with the original heat flux data, as indicated by the negligible standard deviation $(\sigma \approx 0)$ between the reconstructed and original signals. This validation confirms that the leading modes (Modes 1–4) are sufficient to reproduce the primary heat flux dynamics, demonstrating the robustness of the POD methodology and its ability to decompose and interpret complex plasma behaviour.

8. Discharge Groupings Based on POD Characteristics

To characterise the effectiveness of the POD analysis across different W7-X discharges, we propose grouping the discharges based on key features of their POD results:

- Single-mode dominated discharges: in these discharges, the first POD mode captures an overwhelmingly large fraction of the variance (typically $>80\% - 90\%$). Higher-order modes carry only minor residual variance. Such a single-mode structure often occurs under steady conditions with no strong evolving asymmetries—for example, either a largely symmetric heat flux distribution or a fixed asymmetric pattern that persists throughout the discharge. In single-mode cases, the POD essentially identifies one dominant spatial pattern (e.g. the baseline heat flux profile), and the temporal coefficient of that mode captures the bulk of the dynamics (often just a gradual rise or fall in overall heatflux intensity). These discharges tend to show weak correlations between the POD coefficients and plasma parameters; since the divertor heat flux pattern remains relatively stable, changes in density or current have little distinguishable effect on the single dominant mode. The average symmetrisation parameter (ς) in this group can vary: if the single dominant mode is symmetric, ς will be near zero (balanced upper/lower heat load), whereas if the mode is inherently asymmetric, ς will be significantly positive or negative indicating a persistent divertor load asymmetry.
- Multi-mode (two-mode) discharges: these discharges exhibit a richer structure where the first two POD modes each contribute a significant portion of the variance (for example, Mode 1 on the order of $50\%-80\%$ and Mode 2 capturing an additional $20\%-40\%$). The cumulative contribution of the first two modes is high (often $90\%-95\%$), indicating that a two-mode superposition is needed to

describe the divertor heat flux dynamics. This typically corresponds to cases with evolving or more complex asymmetries: for instance, a discharge where the heat flux distribution shifts over time due to changing plasma conditions will require one mode for the base pattern and a second mode to capture the shifting or oscillatory component. Multi-mode discharges generally show stronger correlations between POD temporal coefficients and external plasma parameters. A common scenario (as seen in our analysis) is that the first mode's coefficient correlates with the global density evolution (reflecting density-driven changes in overall heat flux patterns), while the second mode's coefficient correlates with the plasma current evolution (reflecting topology changes that introduce asymmetry). In these cases, the presence of two significant modes indicates an interplay of at least two physical processes. The symmetrisation parameter ς in two-mode discharges is often moderate—the dynamic interplay tends to prevent one divertor side from always dominating. For example, the lower divertor may receive more heat early on and the upper divertor later, resulting in an average ς closer to zero despite the instantaneous asymmetries. Thus, multi-mode discharges often hover around a balanced average ($|\varsigma|$ moderate), in contrast to single-mode asymmetric cases which if asymmetries occur will maintain a large $|\varsigma|$ throughout.

- Higher-mode or complex cases (rare): in our dataset, higher modes beyond the first two carry only minimal variance (each $< 10\%$). We did not identify any discharge that fundamentally required more than two modes for a qualitative description. In principle, however, a discharge with very transient or oscillatory behaviour might spread variance across several modes (none overwhelmingly dominant). Such a case would fall into a 'complex' group where no single mode or two-mode combination captures as much as 90%. These would likely coincide with non-stationary phenomena (e.g. cyclic oscillations or abrupt events), and the POD might yield several modes of comparable weight. In our W7-X survey, no discharge fell clearly into this category—even the most dynamic scenarios were adequately described by two significant modes—but we note it as a potential grouping for more complex future datasets.

In figure 14, we illustrate the proposed groupings by plotting each analysed discharge in terms of two representative features: the dominance of the first mode (x-axis) and the strength of correlation with a key plasma parameter (y-axis). As described, single-mode dominated discharges congregate on the right side of the plot, where $>80\%$ of the variance is in Mode 1. These points (shown as square markers) generally have low correlation coefficients (clustered around the y-axis), reflecting the fact that their sole dominant mode does not track plasma parameter changes strongly. In contrast, the two-mode discharges (circular markers) appear toward the left with a somewhat lower first-mode fraction ($\sim 50\% - 80\%$) and typically more varied correlation values. The colouring of the

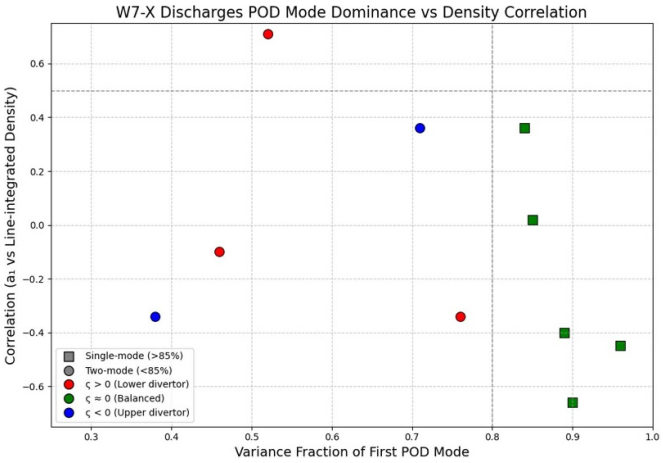

Figure 14. Scatter plot of multiple W7-X discharges in a feature space defined by POD mode dominance and correlation strength. The x-axis is the variance fraction captured by the first POD mode, indicating whether a single mode dominates the heat flux pattern. The y-axis is the Pearson correlation coefficient (r) between the first mode's temporal coefficient (a_1) and the line-integrated electron density (n_e). Each point represents a discharge. Squares denote single-mode dominated discharges (first mode $>80\%$ variance), while circles denote two-mode discharges. The points are further coloured by the average symmetrisation parameter (ς) to indicate divertor heat load balance: red points have positive ς (lower divertor receives more heat on average), blue points have negative ς (upper divertor receives more heat), and green points are near $\varsigma \approx 0$ (symmetrically balanced).

points provides additional insight into divertor asymmetry: for instance, nearly all the single-mode points are green (indicating that their time-averaged ς is small), whereas many two-mode points appear red or blue (indicating a persistent bias to one divertor). This suggests that single-mode discharges generally maintain stable, symmetrical heat flux distributions, while two-mode discharges tend to exhibit dynamic asymmetries that shift the divertor load toward one side consistently throughout the discharge. Overall, this feature-space visualisation supports the qualitative grouping: Group I (single-mode, squares) represents stable patterns with a single dominant mode and typically balanced loads, whereas Group II (two-mode, circles) includes more dynamically evolving discharges characterised by dual-mode structures and persistent divertor asymmetries. This grouping approach is preliminary but provides a useful map of when the POD method yields simple vs multi-faceted descriptions of the divertor heat flux.

Essentially, by examining metrics like the fraction of variance in the first mode, the cumulative contribution of the first two modes, the correlations of mode coefficients with plasma parameters, and the symmetrisation parameter (ς), we can distinguish different types of divertor heat flux behaviour.

For example, some discharges are dominated by a single spatial mode with only minor higher-order contributions, indicating a largely static or equilibrium heat flux pattern, whereas others distribute their variance across two significant modes, signalling more complex or evolving patterns. In

Table 1. Survey of W7-X discharges analysed in this work. For each pulse we list the magnetic-configuration category (edge rotational-transform setting), injected ECRH power P_{ECRH}, the peak line-integrated density $\int n\,\mathrm{d}l_{\max}$, and the pulse duration t_{dur}. 'Standard' denotes the quasi-isodynamic baseline; alternative settings (e.g. Low iota, iota scan, High Mirror) are included to test methodological robustness.

Discharge	Mag.Config.	P_{ECRH}	$\int n\mathrm{d}l_{\max}$	t_{dur}
20 180 816.10	Standard	3.2 MW	$4.7\,\mathrm{m}^{-2}$	15.0 s
20 180 828.30	Low iota	2.5 MW	$3.9\,\mathrm{m}^{-2}$	20.0 s
20 181 010.11	Standard	4.5 MW	$8.1\,\mathrm{m}^{-2}$	8.0 s
20 181 010.22	Standard	4.5 MW	$4.7\,\mathrm{m}^{-2}$	12.0 s
20 181 010.38	Standard	5.5 MW	$12.0\,\mathrm{m}^{-2}$	9.6 s
20 181 016.04	Standard	3.5 MW	$6.5\,\mathrm{m}^{-2}$	10.0 s
20 181 016.06	Standard	5.9 MW	$12.0\,\mathrm{m}^{-2}$	9.0 s
20 181 016.38	Standard	4.0 MW	$8.0\,\mathrm{m}^{-2}$	6.0 s
20 181 017.24	Iota scan	2.0 MW	$6.0\,\mathrm{m}^{-2}$	3.0 s
20 181 017.25	Standard	4.0 MW	$11.5\,\mathrm{m}^{-2}$	37.0 s
20 181 017.41	Standard	5.5 MW	$5.5\,\mathrm{m}^{-2}$	5.0 s
20 230 222.16	High mirror	4.5 MW	$14.0\,\mathrm{m}^{-2}$	14.0 s

the latter, the first mode often represents a baseline symmetric component while the second mode captures an asymmetric deviation or temporal shift in the strike-line distribution. We find that these two-mode discharges tend to occur when there are changes during the discharge (for instance, a ramp in density or a shift in edge current), as evidenced by strong correlations between the POD coefficients and those changing parameters. In contrast, discharges without significant profile evolution (steady-state conditions) often fall into the single-mode category, where POD yields essentially one salient mode that mirrors the time-invariant spatial distribution of heat flux. This mode grouping is reflected in the symmetrisation metric as well, a discharge with a persistent top-bottom asymmetry (large $|\varsigma|$) typically shows that asymmetry captured in one dominant POD mode, whereas discharges with time-varying asymmetry tend to require multiple modes yet may have a smaller average ς.

If a discharge falls into the single-mode dominated group, the implication is that the divertor heat-load pattern is governed by one primary effect (e.g. a stable magnetic topology configuration or a constant drift-induced asymmetry) and that the POD, while still providing a compact representation, may not reveal more than what one could observe directly. In these situations, additional modes or correlations do not contribute much, and the POD analysis serves mainly to confirm that the divertor heat flux was steady or symmetric (or persistently skewed) throughout that shot. On the other hand, if a discharge is grouped as a two-mode case, the POD analysis has teased apart two concurrent phenomena, for example, a baseline heat distribution and a superposed shifting component tied to density or current changes. In such cases, POD proves highly valuable, as it not only compresses the data but also separates different physical processes. We emphasise that this classification is exploratory and introduced in this article as an initial guide. It lays the groundwork for more targeted analyses, for instance, the investigation within a given magnetic configuration how discharges transition from single- to two-mode behaviour as heating or fuelling is varied. A detailed, configuration-by-configuration study is beyond our present scope and will be addressed in future work. Here, our intention is to introduce the concept and demonstrate its promise: even with a modest set of 12 discharges presented in table 1, one can begin to see patterns in when POD yields one dominant mode versus two, and how that correlates with plasma conditions.

9. Conclusion

In this study, a total of twelve discharges spanning multiple magnetic configurations were analysed using the POD method. The primary criterion for discharge selection was the presence of stable ECRH power throughout the pulse. This ensured that the temporal evolution captured by the POD modes could be attributed to intrinsic plasma dynamics and magnetic topology effects, rather than external heating modulations. While the POD method provides a powerful tool for distilling divertor heat-flux data, it is important to acknowledge its limitations and the scope of its applicability. One limitation is evident in cases of single-mode dominance: when essentially one mode encapsulates the entire behaviour of the system, the POD analysis does not uncover multiple independent features, it reduces the data to a trivial single degree of freedom. In such cases, the insight gained is limited. Another limitation is that POD, by construction, prioritises modes by variance rather than by physical meaningfulness. Thus, there may exist lower-variance yet physically coherent structures (for example, a small oscillatory hotspot or a subtle fluctuation) that are relegated to higher modes or even obscured entirely by the dominance of larger-variance patterns. In other words, POD can miss or deemphasise phenomena that are important but energetically small. A related point is the sensitivity of POD to signal-to-noise levels: noise or random fluctuations, if pervasive, will contribute to the overall variance and can mix into the POD modes, sometimes making the interpretation of higher-order modes ambiguous. We have taken care in our data conditioning (e.g. subtracting background levels and focusing on steady phases of the discharge) to mitigate spurious effects. It is worth emphasising that one of the inherent strengths of the

POD method lies in its robustness to uncorrelated noise. Since POD extracts coherent spatial and temporal patterns based on variance, random fluctuations tend to average out across the time basis and are effectively excluded from the dominant modes. Consequently, the leading POD modes are largely unaffected by residual noise, while small-scale uncorrelated perturbations are relegated to higher-order modes with negligible eigenvalue contributions. Although the signal-to-noise ratio always plays a role in any diagnostic process, the POD algorithm intrinsically suppresses incoherent noise, and this property has been exploited in previous applications. In this work, we have qualitatively noted this behaviour, and a more systematic sensitivity analysis, exploring how mode structure evolves with noise filtering, temporal window selection, or data resolution, will be addressed in a future study.

Diagnostic Uncertainty and POD Robustness: The IR thermography system used to determine divertor heat flux carries an estimated uncertainty in absolute magnitude of approximately 10%, primarily due to calibration errors and repeatability. It is important to stress, however, that this diagnostic uncertainty does not directly propagate into the POD in a linear or quantitative manner. POD inherently identifies dominant spatial-temporal structures based on coherent variance within the dataset and tends to suppress uncorrelated noise by relegating it to higher-order modes with negligible eigenvalues. Thus, the impact of diagnostic uncertainty on the leading POD modes is expected to be minimal. While a precise quantification of POD uncertainty is non-trivial and seldom addressed in the literature, we implemented a didactic sensitivity analysis to estimate its effect. The input matrix was perturbed by $\pm 10\%$, and the POD was recomputed to assess the variation in explained variance (λ_i), spatial mode structures, and temporal coefficients. The results indicate that the relative changes in the leading mode variances were negligible. The detailed results are summarised in the table 2 below. These results confirm that the leading POD modes are extremely robust to reasonable variations in input magnitude, and that the uncertainty introduced by the diagnostic system does not affect the integrity of the extracted dominant structures. It follows that fluctuations or asymmetries detected in the primary modes, particularly those exceeding a few percent, are unlikely to result from instrumental noise and can be interpreted as physically meaningful. The present results therefore reflect the features that consistently emerge across modes and discharges. Although a rigorous uncertainty propagation remains an open challenge, we highlight that the lack of such analyses in the existing literature is not due to irrelevance but rather due to the intrinsic methodological difficulty. It is generally accepted that the accuracy of POD results is fundamentally constrained by the accuracy and richness of the underlying data. This consideration, however, further strengthens the conclusions drawn here, given the excellent internal consistency and mode separation observed.

One complementary approach we foresee to overcome some of POD's limitations is the application of dynamic mode decomposition (DMD) alongside POD. DMD is a data-driven decomposition technique that, unlike POD, is expressly designed to identify modes associated with specific oscillation frequencies. Each DMD mode is characterised by a fixed frequency and thus can directly capture coherent oscillatory behaviour that might be smeared across multiple POD modes. DMD could help detect and characterise cyclic or periodic heat-flux patterns that are not immediately obvious from the POD analysis alone. We suggest that a combined application of POD and DMD would provide a more complete picture of the heat-flux dynamics: the POD excels at capturing the dominant spatial distribution of heat loads and overall energy content, while the DMD would be able to pinpoint any underlying periodicities in time and attribute them to distinct modes. Together, these methods could cross-validate each other.

Table 2. Sensitivity of POD mode parameters to $\pm 10\%$ perturbations in input data. Changes in explained variance (λ) are reported as relative differences, and correlations of spatial and temporal modes are reported as Pearson coefficients.

Mode	$\Delta\lambda_{-10\%}$ [%]	$\Delta\lambda_{+10\%}$ [%]	$r_{\text{spatial}}^{\pm 10\%}$	$r_{\text{temp}}^{\pm 10\%}$
λ_1	$2{,}1 \times 10^{-14}$	$1{,}5 \times 10^{-13}$	1.0	1.0
λ_2	$-1{,}6 \times 10^{-14}$	$-1{,}8 \times 10^{-13}$	1.0	1.0
λ_3	$-4{,}1 \times 10^{-14}$	$8{,}2 \times 10^{-14}$	1.0	1.0
λ_4	$-2{,}5 \times 10^{-13}$	$-1{,}3 \times 10^{-13}$	1.0	1.0

The results of the first time application of the Karhunen–Loéve expansion on the heat flux distributions, presented in this study demonstrates the effectiveness of POD as a useful tool for analysing and interpreting the complex dynamics of plasma. By isolating the dominant spatial and temporal modes, the POD method provided valuable insights into the asymmetries and transport phenomena governing heat deposition on the divertor surfaces. The introduction of the average symmetrisation parameter *(*ς*)* further enhanced the analytical framework, offering a quantitative measure of the heat flux asymmetry between the upper and lower divertors. This parameter not only highlighted the physical significance of drift-induced transport but also established a clear metric for assessing divertor performance under varying plasma conditions.

The correlation analysis revealed compelling connections between the POD temporal coefficients and key plasma parameters, notably the strong association between the first two coefficients $a_1(t)$ with the line-integrated electron density, and $a_2(t)$ with the toroidal plasma current. These findings point to a division of physical effects across multiple modes, suggesting that steady-state and dynamic behaviours in plasma transport can be distinguished and separately analysed. This example of the use of POD demonstrates the ability of POD to decompose the simultaneous influence of several plasma parameters on the heat flux.

The reconstruction of heat flux signals validated the POD methodology by accurately reproducing the observed data while preserving the key spatial and temporal features. This reconstruction underscored the multiscale nature of heat flux dynamics, demonstrating how dominant and higher-order modes interact to create the observed patterns of asymmetry.

The combined use of reconstruction, symmetrisation analysis, and parameter correlations provided an overview of plasma-edge interactions, in the stellarator magnetic configurations.

The validation of these findings with a second discharge, 20 180 816.010 (corresponding figures presented in appendix), further reinforces the reliability and applicability of the proposed methodologies. The asymmetries in the given discharge have been chosen to me more dominant on the upper divertor, in order to serve as a testbed for the robustness of the POD analysis and the symmetrisation parameter. The results demonstrated consistency with the primary discharge, confirming that the observed physical effects and analytical insights are not specific to a single plasma scenario but hold broader significance across varying operational conditions.

In summary, this study highlights the potential of POD and the average symmetrisation parameter as powerful tools for exploring and optimising divertor heat flux dynamics in stellarator-type fusion devices. By bridging the gap between experimental observations and theoretical models, this approach provides a pathway for improving PFC performance and advancing the operational capabilities of the W7-X and similar fusion reactors.

This work presents the first application of the POD method to the analysis of heat flux data acquired via IR camera measurements. While the toroidal current is the dominant factor-shifting the magnetic island and consequently altering the heat flux distribution on the divertor-we also observed correlations with other plasma parameters, such as plasma density and W_{dia}. Although a more detailed examination of these correlations is beyond the scope of this paper and will be addressed in future work, our analysis demonstrates that POD can effectively capture the interplay of multiple plasma parameters.

Data availability statement

The data cannot be made publicly available upon publication because they are not available in a format that is sufficiently accessible or reusable by other researchers. The data that support the findings of this study are available upon reasonable request from the authors. https://w7x-logbook.ipp-hgw.mpg.de/.

Acknowledgments

This work has been carried out within the framework of the EUROfusion Consortium, funded by the European Union via the Euratom Research and Training Programme (Grant Agreement No 101052200 EUROfusion). Views and opinions expressed are however those of the author(s) only and do not necessarily reflect those of the European Union or the European Commission. Neither the European Union nor the European Commission can be held responsible for them.

The project is co-financed by the Polish Ministry of Education and Science under the program ‘Co-Financed International Projects.’

Appendix

In addition to the primary analysis of discharge 20 180 828.030, further validation was performed on discharge 20 180 816.010, which is in the standard magnetic configuration, to verify the reproducibility of the POD framework. As illustrated in figures 15 and 16 in appendix, the time-averaged divertor heat flux distribution and its associated data matrix exhibit characteristics similar to those observed in the primary discharge (cf figures 4 and 7). The percentage contribution of the POD modes, presented in figure 8 for the primary discharge and figure 17 for the validation discharge, consistently demonstrates that the first two modes capture the bulk of the total variance-thereby corroborating the dimension-reduction efficacy of the POD method. Moreover, the spatial modes and temporal coefficients obtained from the primary analysis (figures 9 and 10) are reflected in figures 18 and 19, respectively, indicating that the dominant heat flux patterns and their evolution are robust across different discharges. The average symmetrisation parameter, which quantifies the asymmetry between the upper and lower divertor heat fluxes, is also consistent between the two discharges (compare figures 11 and 20), affirming that the underlying drift-induced transport phenomena are reliably captured. Furthermore, the correlation scatter plots (figures 12 and 21) reveal similar strong associations between the POD temporal coefficients and key plasma parameters such as line-integrated electron density and toroidal plasma current. Finally, the reconstructed heat flux profiles (figures 13 and 22) exhibit near-perfect agreement with the original signals, thereby validating the overall POD decomposition. Collectively, these extended results substantiate that the POD method, along with the Average Symmetrisation parameter, robustly captures the essential features of divertor heat flux dynamics across varying plasma conditions, thus enhancing its applicability for predictive modelling in stellarator-type fusion devices.

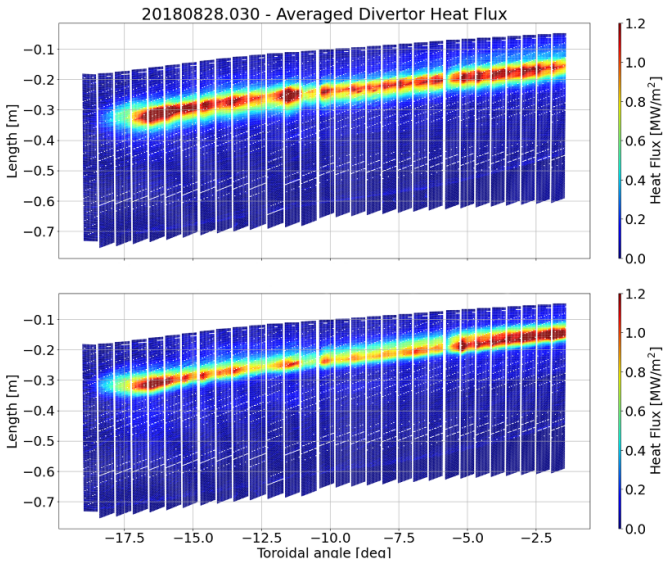

Figure 15. Time-averaged divertor heat flux distribution for discharge 20 180 816.010.

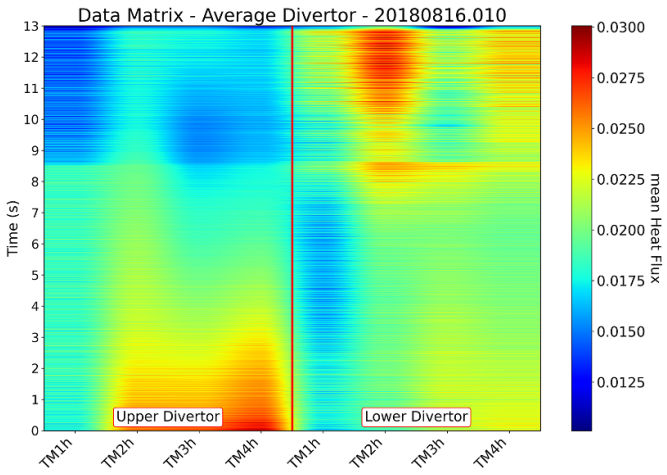

Figure 16. Data Matrix of 20 180 816.010 for POD Analysis of Mean heat flux.

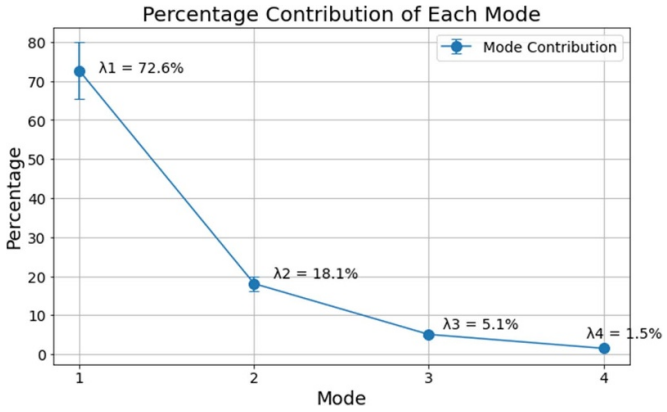

Figure 17. The percentage contribution $\lambda_k / \sum_{i=1}^{n}$ across various POD modes for the 20 180 816.010 discharge.

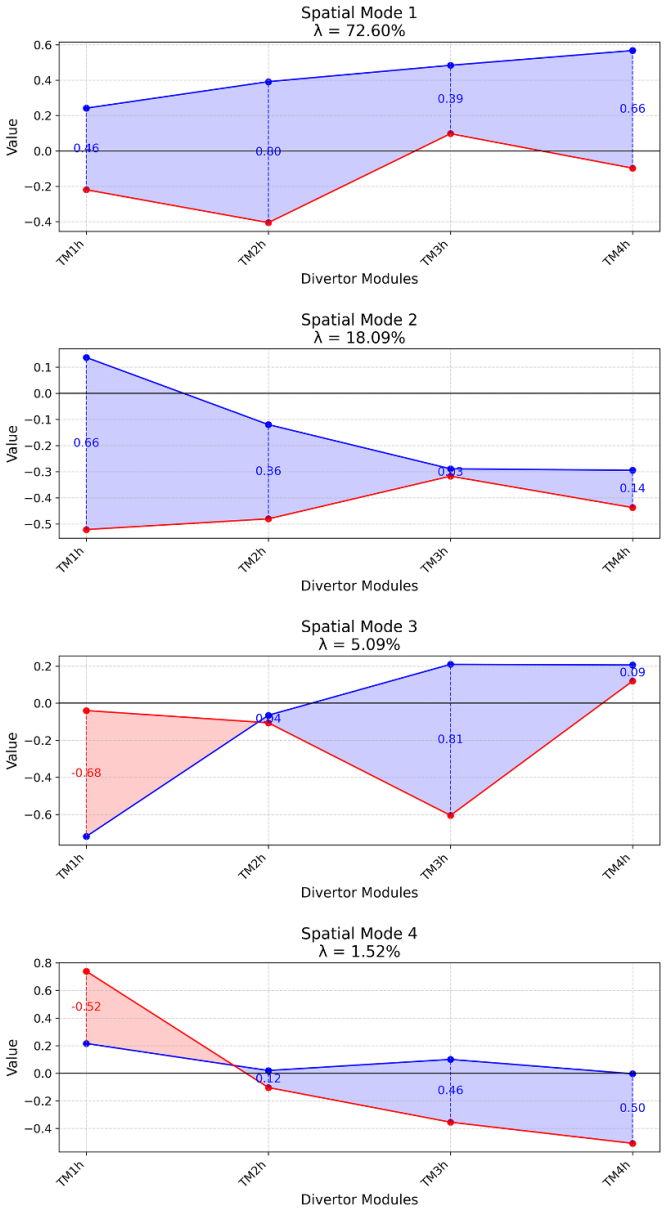

Figure 18. Spatial modes derived from the POD analysis for discharge 20 180 816.010.

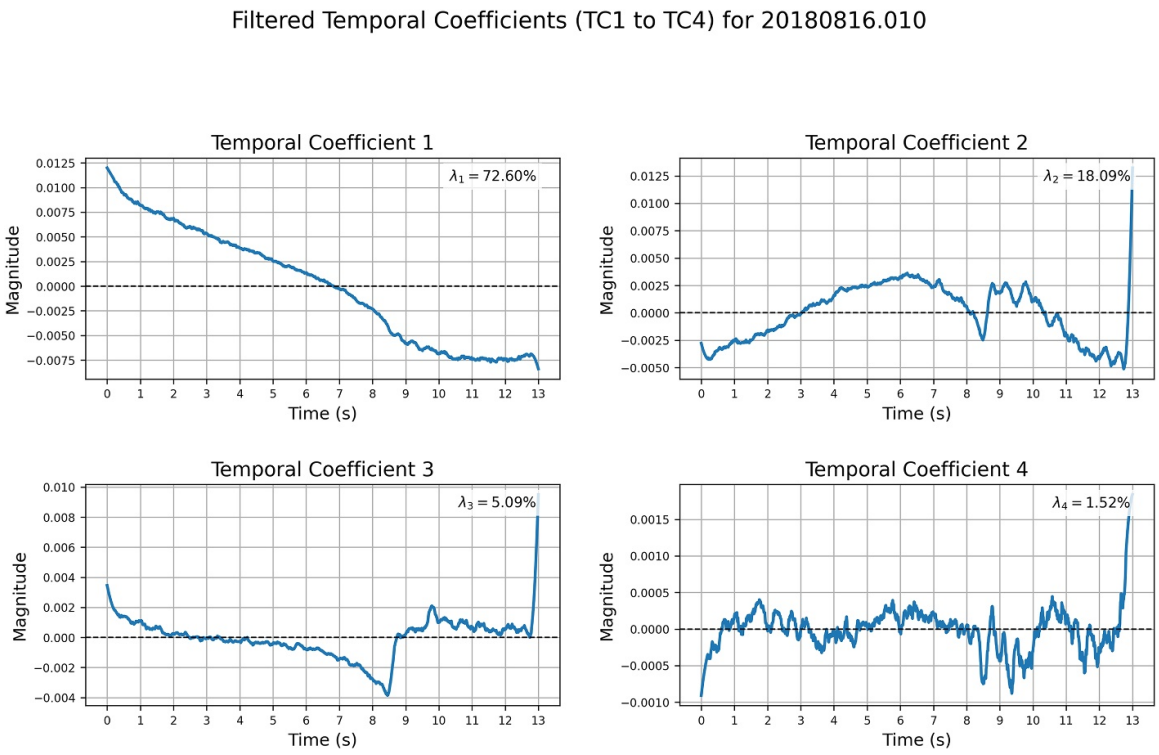

Figure 19. Temporal coefficients derived from the POD analysis for discharge 20 180 816.010.

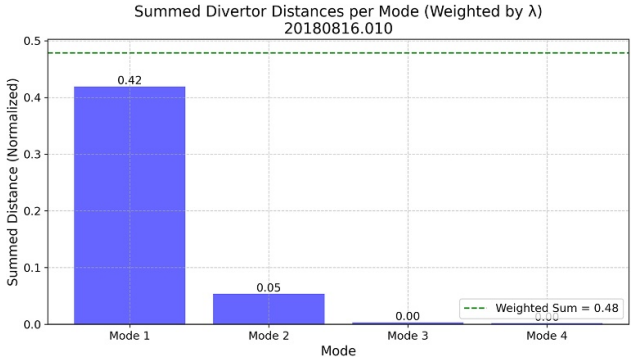

Figure 20. Average symmetrisation parameter (ς) per mode, for discharge 20 180 816.010.

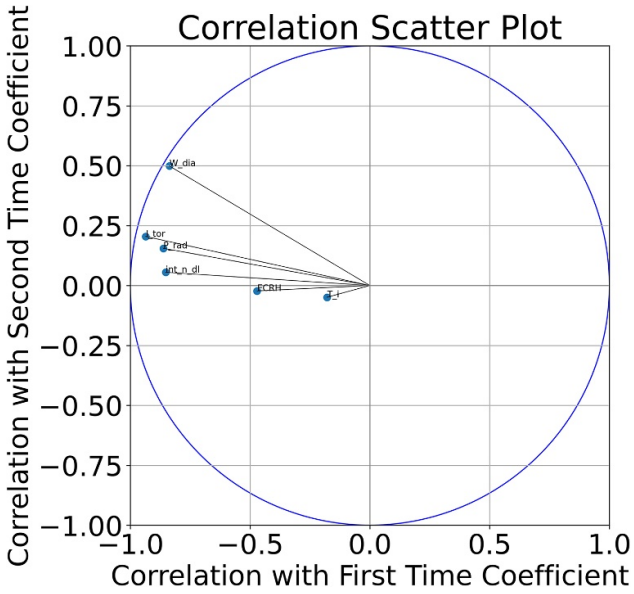

Figure 21. Correlation scatter plot between plasma parameters and the first two temporal coefficients from POD analysis of discharge 20 180 816.010.

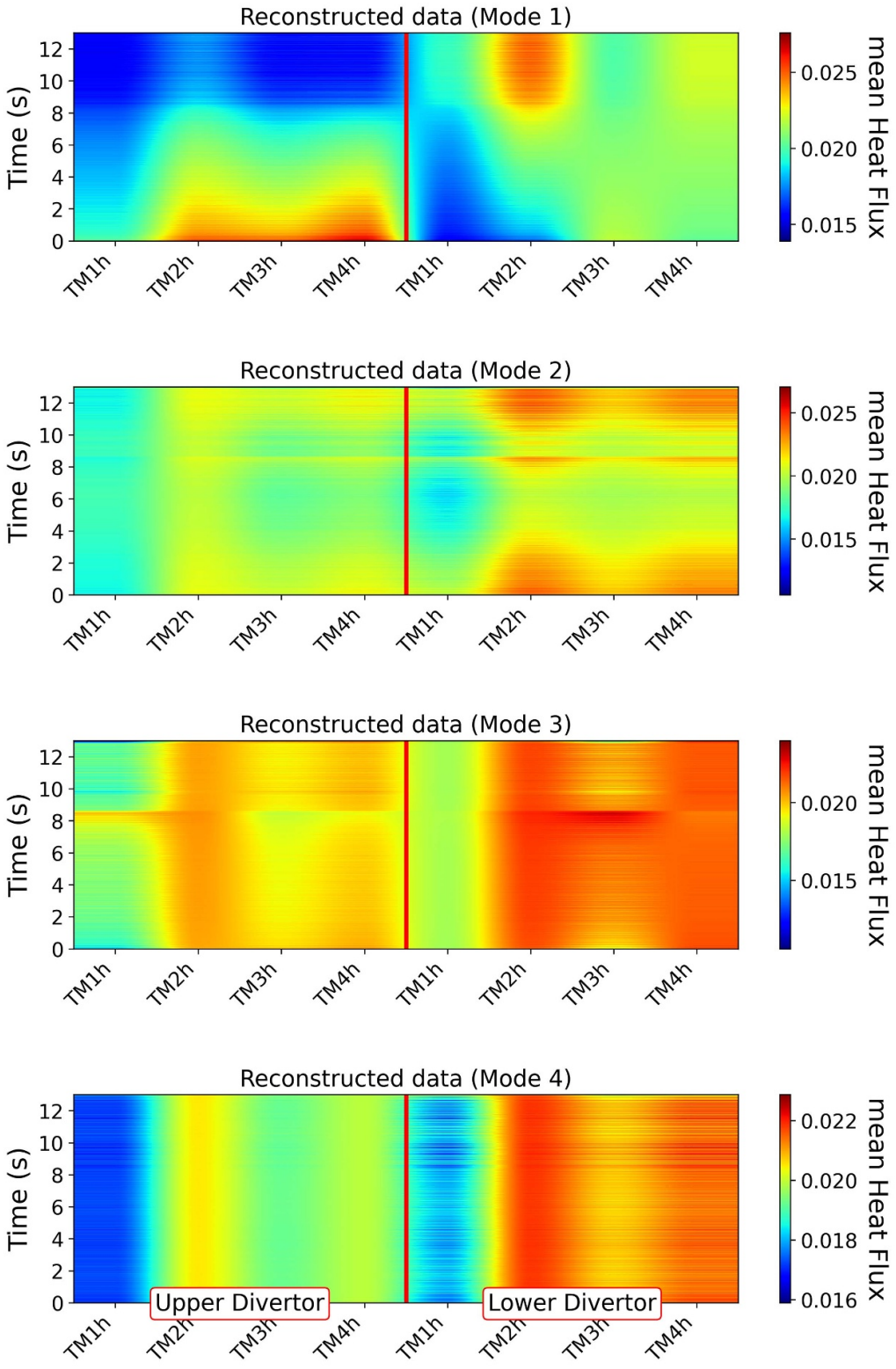

Figure 22. Reconstructed heat flux data for the first four POD modes for discharge 20 180 816.010.

ORCID iDs

Bartosz Zamorski 0000-0003-0441-6516
Marcin Sleczka 0000-0003-0592-5611
Marcin Jakubowski 0000-0002-6557-3497
Yu Gao 0000-0001-8576-0970
Aleix Puig Sitjes 0000-0002-4733-6068
Konrad Czerski 0000-0002-8625-2481

References

Andreeva T *et al* 2022 Magnetic configuration scans during divertor operation of Wendelstein 7-X *Nucl. Fusion* **62** 026032
Berkooz G, Holmes P and Lumley J L 1993 The proper orthogonal decomposition in the analysis of turbulent flows *Annu. Rev. Fluid Mech.* **25** 539–75
Boscary J, Ehrke G, Greuner H, Junghanns P, Li C, Mendelevitch B, Springer J and Stadler R 2021 Completion of the production of the W7-X divertor target modules *Fusion Eng. Des.* **166** 112293
Corre Y *et al* 2021 Thermographic reconstruction of heat load on the first wall of Wendelstein 7-X due to ECRH shine-through power *Nucl. Fusion* **61** 066002
Feng Y, Sardei F, Grigull P, McCormick K, Kisslinger J and Reiter D 2006 Physics of island divertors as highlighted by the example of W7-AS *Nucl. Fusion* **46** 807–19
Gan K F, Ahn J-W, Park J-W, Maingi R, McLean A G, Gray T K, Gong X and Zhang X D 2013 2D divertor heat flux distribution using a 3D heat conduction solver in National Spherical Torus Experiment Available *Rev. Sci. Instrum.* **84** 023505
Gao Y *et al* 2019 Methods for quantitative study of divertor heat loads on W7-X *Nucl. Fusion* **59** 066007
Grulke O *et al* 2024 Overview of the first Wendelstein 7-X long pulse campaign with fully water-cooled plasma facing components *Nucl. Fusion* **64** 112002
Hammond K C *et al* 2019 Drift effects on W7-X divertor heat and particle fluxes *Plasma Phys. Control. Fusion* **61** 125001
Herrmann A, Junker W, Gunther K, Bosch S, Kaufmann M, Neuhauser J, Pautasso G, Richter T and Schneider R 1995 Energy flux to the ASDEX-Upgrade diverter plates determined by thermography and calorimetry *Plasma Phys. Control. Fusion* **37** 17–29
Jakubowski M *et al* 2021 Overview of the results from divertor experiments with attached and detached plasmas at Wendelstein 7-X and their implications for steady-state operation *Nucl. Fusion* **61** 106003
Jauregi E *et al* 2003 Turn-key supply for the power supplies of the control coils of wendelstein 7-X experiment *Fusion Eng. Des.* **66–68** 1125–32
Klinger T *et al* 2019 Overview of first Wendelstein 7-X high-performance operation *Nucl. Fusion* **59** 112004
Kriete D M *et al* 2023 Effects of drifts on scrape-off layer transport in W7-X *Nucl. Fusion* **63** 026022
Landreman M J 2011 *PhD Thesis* Massachusetts Institute of Technology
Lazerson S A *et al* 2018 Error fields in the Wendelstein 7-X stellarator *Plasma Phys. Control. Fusion* **60** 124002
McCormick K *et al* 2003 Island divertor experiments on the Wendelstein 7-AS stellarator *J. Nucl. Mater.* **313–316** 1131–40
Mendez M A, Balabane M and Buchlin J-M 2019 Multi-scale proper orthogonal decomposition of complex fluid flows *J. Fluid Mech.* **870** 988–1036
Niemann H *et al* 2020a Large wetted areas of divertor power loads at Wendelstein 7-X *Nucl. Fusion* **60** 084003
Niemann H *et al* 2020b Features of near and far scrape-off layer heat fluxes on the Wendelstein 7-X inboard limiters *Nucl. Fusion* **60** 016014
Pearson K 1901 LIII. On lines and planes of closest fit to systems of points in space *London, Edinburgh Dublin Phil. Mag. J. Sci.* **2** 559–72
Pedersen T S *et al* 2019a First results from divertor operation in Wendelstein 7-X *Plasma Phys. Control. Fusion* **61** 014035
Pedersen T S *et al* 2019b First divertor physics studies in Wendelstein 7-X *Nucl. Fusion* **59** 096014
Pisano F *et al* 2020 Tools for image analysis and first wall protection at W7-X *Fusion Sci. Technol.* **76** 933–41
Pisano F, Cannas B, Fanni A, Sias G, Gao Y, Jakubowski M, Niemann H and Puig Sitjes A 2021 Learning control coil currents from heat-flux images using convolutional neural networks at Wendelstein 7-X *Plasma Phys. Control. Fusion* **63** 025009
Puig Sitjes A *et al* 2021 Real-time detection of overloads on the plasma-facing components of Wendelstein 7-X *Appl. Sci.* **11** 11969
Rummel T, Rißе K, Nagel M, Mönnich T, Schneider M, Füllenbach F and Bosch H-S 2019 Wendelstein 7-X magnets: experiences gained during the first years of operation *Fusion Sci. Technol.* **75** 786–93
Sitjes A P *et al* 2018 Wendelstein 7-X near real-time image diagnostic system for plasma-facing components protection *Fusion Sci. Technol.* **74** 116–24
Śleczka M *et al* 2018 Modulation of the strike line position using control coils in Wendelstein 7-X *45th EPS Conf. on Plasma Physics*
Tanaka H *et al* 2018 Analysis of indefinite divertor footprint with proper orthogonal decomposition in hydrogen/deuterium plasmas in LHD *Plasma Phys. Control. Fusion* **60** 125001
Tanaka H, Masuzaki S, Kawamura G, Kobayashi M, Suzuki Y, Morisaki T and Ohno N Characterized divertor footprint profile modification with the edge pressure gradient in the Large Helical Device 2019 *Nucl. Mater. Energy* **19** 378–83
Wurden G A *et al* 2018 A divertor scraper observation system for the Wendelstein 7-X stellarator *Rev. Sci. Instrum.* **89** 10E102